DEVELOPMENT OF DUAL CO_2 LASER INTERFEROMETER FOR LARGE TOKAMAK

March 1995

Yasunori KAWANO, Akira NAGASHIMA, Takaki HATAE and Soichi GUNJI

日 本 原 子 力 研 究 所
Japan Atomic Energy Research Institute

Development of Dual CO_2 Laser Interferometer for Large Tokamak

Yasunori KAWANO, Akira NAGASHIMA, Takaki HATAE
and Soichi GUNJI

Department of Fusion Plasma Research
Naka Fusion Research Establishment
Japan Atomic Energy Research Institute
Naka-machi, Naka-gun, Ibaraki-ken

A new CO_2 Laser interferometer has been developed to measure electron density of tokamak plasmas. Two different wavelength oscillators of 10.6 μm and 9.27 μm are utilized for simultaneous measurement of the density component and the optical path length change. A new technique of the common use of a frequency shifter for two color lasers improves the stability of the system by a complete matching of both beat frequencies. The system has advantages on practical problems of window darkening, large mechanical vibrations of reflection mirrors, monitoring of laser beams and simplified the optical layout design by using the close wavelength. The electron density of JT-60U plasma is successfully measured up to a plasma current of 3 MA. The density behavior of fast major disruptions are also diagnosed without a fringe loss. The effective density resolution is observed as 2×10^{19} m^{-2}, which corresponds to about a 1/10 fringe. An ultra high resolution (1/10^4 fringe) phase comparator has been developed to improve the density resolution of the dual CO_2 system. Achieved performance shows the feasibility of the dual CO_2 laser interferometer for future large devices such as ITER.

大型トカマクのためのデュアルＣＯ₂レーザ干渉計の開発

日本原子力研究所那珂研究所炉心プラズマ研究部

河野　康則・長島　　章・波多江仰紀・軍司　操一

　大型トカマクにおける電子密度計測を目的とした新しいＣＯ₂レーザ干渉計を開発した。この干渉計は，異なる波長（10.6μm及び9.27μm）の2つのＣＯ₂干渉計により，電子密度成分と光路長変化成分の同時測定を行うものである。また周波数シフタの共用化により，両者の干渉ビート周波数を一致させ，装置の安定性向上を得ている。特長としては，真空窓の汚れや反射ミラー振動の影響の低減化，比較的単純な光学部品構成の実現，等が挙げられる。これまでＪＴ－６０Ｕの実験において，プラズマ電流3ＭＡまでの電子密度を測定することができた。また，ディスラプション時における密度挙動をフリンジロスなしに計測することに成功した。実効的な密度分解能は2×10^{19}m^{-2}（1/10フリンジに相当）であった。また密度分解能をさらに改善するために，1/10⁴フリンジ分解能の超高分解能位相比較器を開発中である。今回達成された成果は，デュアルＣＯ₂レーザ干渉計のＩＴＥＲなど将来の大型装置における実現性を示したものといえる。

那珂研究所：〒311-01　茨城県那珂郡那珂町大字向山８０１－１

目　　　　次

Contents

1. Introduction

To measure electron density of plasmas with sufficient reliability is one of the key issues of tokamak fusion research. The laser interferometry has been playing an important role in this field and it is further expected to be essential in future large devices such as ITER (International Thermonuclear Experimental Reactor). In ITER, a CO_2 laser interferometer is proposed for the electron density monitor and for absolute density calibration of LIDAR [1]. This choice will eliminate the refraction effect by a dense and large plasma, Faraday rotation due to the large magnetic field especially in the case of a tangential chord. On the other hand, with a light source of shorter wavelength, optical transmission problem becomes more serious for mirrors and windows. The CO_2 laser of 10.6 μm is a suitable light source for the interferometer neglecting the problems of these effects and commercial availability. To complete the density measurement by interferometry requires simultaneous measurement at a different wavelength along the same optical path in order to compensate optical path length changes due to mirror vibration and displacement. For this purpose, combination with an IR-HeNe laser (3.39 μm) was proposed [1].

For the interferometer of JT-60U, we have examined the 10.6 μm and 3.39 μm combination system for a toroidally tangent line of sight [2, 3], which is very similar to the ITER proposal. This configuration was introduced for the central density measurement of the " high βp H mode " plasmas in JT-60U, which made the world record of the fusion triple product of 1.1×10^{21} $m^{-3} \cdot s \cdot keV$ [4-6].

However, we found several problems in the operation of this combination as follows; (1) there were many missing fringes and jumps on data of the IR-HeNe interferometer with plasma current exceeding 2 MA or with a rapid change of the plasma position. This is because of the probing laser beam of the IR-HeNe shifting out of the detector due to a displacement or a mirror vibration. (2) The darkening of windows and mirrors decreased the returned IR-HeNe intensity. The signal to noise ratio becomes smaller. (3) The zero level of a calculated density trace often drifted in a time scale of minutes. This indicates that there was a slight difference between both beat frequencies and/or an unbalanced changing of path length in two interferometers.

These problems must be resolved to obtain data more routinely. The IR-HeNe laser, however, has relatively small output power (8 mW) and it is difficult to increase the power with the needed longitudinal mode. This is a crucial disadvantage in beam handling and detecting in large fusion machines. From this point of view more powerful interferometers are required for large tokamaks.

To achieve this purpose, we have modified the system to a dual CO_2 system which uses close wavelengths of 10.6 μm and 9.27 μm. The system has advantages on practical problems such as ; reduction of the beam transparency of vacuum windows by surface darkening, large mechanical vibration and displacement of reflection mirrors, and laser beam monitoring. Furthermore, the layout of optical components is simplified by using close wavelengths of CO_2 oscillators. A new technique of using a single frequency shifter; AOM (Acoust Optic Modulator) common for different wavelength lasers is also developed. This technique contributes to suppression of the zero level drift by matching both beat frequencies completely.

We have succeeded in measuring the line electron density reliably up to 3 MA plasma. It also enabled us to investigate even a fast major disruption, which was almost impossible with the conventional interferometric system such as with alcohol lasers. The observed density resolution was relatively poor as expected without data smoothing. To resolve this problem we have developed an ultra high resolution phase comparator, with $1/10^4$ fringe resolution and a time response of 1 μs. This resolution is 100 times higher than our conventional phase comparator, and will resolve the difficulty in recognizing small density change.

In this paper, we describe the new interferometer with dual CO_2 combination. The schematic of the system is depicted in section 2. The common use of an AOM to different wavelength lasers is described in section 3. Operation results are presented in section 4. Example of data for the major disruption is presented in section 5. A basic performance of the ultra high resolution phase comparator is shown in section 6. Section 7 is devoted to discussion. A summary is given in section 8.

2. Schematic of interferometer

The dual CO_2 laser interferometer consists of seven major parts ; CO_2 laser oscillators, frequency shifters, relay optics, retardation optics, vacuum windows, detectors, and data acquisition. Relay optics, vacuum windows and data acquisition parts are not changed from the previous system [2, 3].

2.1 Line of sight

Figure 1 shows the laser beam line in the vacuum vessel of JT-60U. Laser beams are launched into the vacuum vessel tangentially through a ZnSe window at an equatorial port. A CCR (Corner Cube Reflector) is installed outside an another ZnSe window, which reflects laser beams with a vertical shift of 15 mm. A laser path length in the plasma is about 6 m (for one way) for a relatively large plasma configuration shown in fig. 1 (a). The tangent radius of the laser path is 3.11 m. With the plasma major radius larger than 3.11 m, the laser beam crosses the plasma central region twice, enhancing the contribution from the plasma center. The diameters of the laser beams are in the range from 12 mm to 17 mm in the vacuum vessel.

2.2 CO_2 laser oscillators, frequency shifters, detectors

CO_2 laser oscillators, frequency shifters and detectors are installed on a vibration isolated bench. Figure 2 shows the arrangement on the bench. CO_2 laser oscillators are model GLD2042 from NEC cooperation with an output power of 10 Watt. Each wavelength is tuned at different branches as 10P(20) with wavelength of 10.6 μm (10.588149 μm) and 9R(20) of 9.27 μm (9.268831 μm) , respectively. The lasing frequency can be stabilized by active feedback control of a cavity length. A piezo transducer at the output mirror and a lock-in stabilizer are used for this purpose [7]. When the stabilizer is working, the laser is called in " the stabilized mode ". Without stabilization, the laser is called in " the free running mode ". A visible HeNe laser (5 mW) is for the alignment of optical axis. Both CO_2 laser beams are divided into two parts. One part is probing beams which travel to the plasma and another is local beams for the heterodyne signal detection.

The center beat frequency of 2 MHz must be chosen in order to satisfy the specification of phase comparators. To produce the 2 MHz beat signal, a couple of AOMs (model 1206B-7 from ISOMET cooperation) is commonly used as a frequency shifter of both CO_2 laser beams. Probing beams of 10.6 μm and 9.27 μm are superimposed at DM1 dichromatic mirror and they receive 40 MHz frequency upshift at AOM1. Local beams are also superimposed at DM2 dichromatic mirror and receive 42 MHz upshift at AOM2. After that, probing beams go into the relay optics and local beams go into the retardation optics.

The returned beams are re-separated into two wavelengths at DM5 and DM6 and filters (FIL1, FIL2). Each 2 MHz beat signal is detected by a room temperature HgCdTe (mercury-cadmium-tellurium) detector with an active area of 2 x 2 mm^2.

2.3 Relay optics, Retardation optics, Vacuum window

The relay optics consists of a flexible light guide, two telescope optics and nine flat mirrors. The probing beams propagate from the vibration isolated bench to the vacuum vessel with a total path length of up to about 50 m to the CCR. The common path mode matching [2] and silver coated mirrors enable this long distance propagation for beams of three wavelengths; 10.6 μm, 9.27 μm and 0.633 μm. Mirror mounts installed at the beam launching port are made of FRP (Fiber Reinforced Plastics) to avoid the electromagnetic force.

The retardation optics is installed near the optical bench on the B1 floor to match the path length of local beams with that of probing beams. The retarded path difference is 39.61 m, which corresponds to the path length from the MB2 (mirror box no. 2) to the CCR. It consists of 13 flat mirrors and a telescope optics which works as the second telescope of the relay optics. The local beams are propagated parallel to the probing beams from the bench to MB2 and are drawn into the retardation optics. After the travel for 39.61 m, local beams are reflected by a CCR installed at the end of the retardation path.

Vacuum windows are made of ZnSe plates (dia. 110 mm x thick 10 mm). Two plates are used at both vacuum ports for safety against a radioactive leak. Initial transparencies of the plate are optimized for the previous laser combination such as; 92 % for 10.6 μm, 95

% for 3.39 μm and 80 % for 0.633 μm, respectively. It was not necessary to modify the specification of these ZnSe plates for a new wavelength of 9.27 μm.

2.4 Signal detection and data acquisition

Figure 3 shows the schematic of signal detection and data acquisition. A probing beam and a local beam are superimposed on the detector surface to produce a 2 MHz interference beat signal. The beat signal is fed through electrical filters and pre-amplifiers and is converted to an optical signal. It is transmitted to the phase comparator through an optical fiber cable. A reference signal is generated from AOM driver signals by a frequency mixer. This signal is also transmitted to the phase comparator and is commonly used as a 2 MHz reference signal for both 10.6 μm and 9.27 μm interferometers. The phase comparator can measure the phase shift with 1/100 fringe resolution by a 200 MHz scale clock. Both phase shift data are stored in a data storage system and the main frame computer (ISP) calculates the line electron density ($\bar{n}_e L_p$) by using eq. (5) in ref. [2] as,

$$\bar{n}_e L_p = -9.01356 \times 10^{20} \, (\, F_{10.6} - F_{9.27} \, / \, 1.14234 \,) \tag{1}$$

where the $\bar{n}_e$ is the line averaged electron density, the L_p is the laser path length in the plasma, $F_{10.6}$ and $F_{9.27}$ denote measured phase shifts of 10.6 μm and 9.27 μm interferometers in unit of fringe, respectively. The maximum sampling rate is 5μsec, which is determined by the capacity of data storage system.

3. Simultaneous frequency shift of different wavelength lasers by single AOM

The phase shift of a probing signal from a reference signal is generally originated by a change of the laser path length (path component) and a change of refractive index related to the electron density (density component). Since both wavelengths of CO_2 lasers are close, it is essential to eliminate phase shifts caused by an unbalanced change of path length and frequency fluctuation of lasers. A minimization of the un-coaxial path part between

% for 3.39 μm and 80 % for 0.633 μm, respectively.　It was not necessary to modify the specification of these ZnSe plates for a new wavelength of 9.27 μm.

2.4　Signal detection and data acquisition

　Figure 3 shows the schematic of signal detection and data acquisition.　A probing beam and a local beam are superimposed on the detector surface to produce a 2 MHz interference beat signal.　The beat signal is fed through electrical filters and pre-amplifiers and is converted to an optical signal.　It is transmitted to the phase comparator through an optical fiber cable.　A reference signal is generated from AOM driver signals by a frequency mixer.　This signal is also transmitted to the phase comparator and is commonly used as a 2 MHz reference signal for both 10.6 μm and 9.27 μm interferometers.　The phase comparator can measure the phase shift with 1/100 fringe resolution by a 200 MHz scale clock.　Both phase shift data are stored in a data storage system and the main frame computer (ISP) calculates the line electron density ($\bar{n}_e L_p$) by using eq. (5) in ref. [2] as,

$$\bar{n}_e L_p = - 9.01356 \times 10^{20} \, (\, F_{10.6} - F_{9.27} \diagup 1.14234 \,) \tag{1}$$

where the $\bar{n}_e$ is the line averaged electron density, the Lp is the laser path length in the plasma,　$F_{10.6}$ and $F_{9.27}$ denote measured phase shifts of 10.6 μm and 9.27 μm interferometers in unit of fringe, respectively.　The maximum sampling rate is 5μsec, which is determined by the capacity of data storage system.

3. Simultaneous frequency shift of different wavelength lasers by single AOM

　The phase shift of a probing signal from a reference signal is generally originated by a change of the laser path length (path component) and a change of refractive index related to the electron density (density component).　Since both wavelengths of CO_2 lasers are close, it is essential to eliminate phase shifts caused by an unbalanced change of path length and frequency fluctuation of lasers.　A minimization of the un-coaxial path part between

interferometers is effective against the unbalanced change in each path. The phase shift due to the frequency fluctuation of lasers can be suppressed by the retardation optics. However, it is also a key issue to match beat frequencies of interferometers as much as possible. It is because a slight beat frequency difference can result in base line drifts on the calculated density trace. To match two beat frequencies, we developed a new technique of a simultaneous frequency shift for different wavelength lasers by a single AOM. Figure 4 shows the alignment of two laser beams for 40 MHz frequency upshift. A medium of the AOM is made of single crystal germanium with a sound speed of 5500 m/s. From a lattice constant (Δx) of 137.5 μm, Bragg angles of the 10.6 μm and the 9.27 μm are determined as 38.55 mrad and 33.72 mrad, respectively. An incident angle of the 10.6 μm beam is set at its Bragg angle. Therefore the output angle is also the Bragg angle. This is the best condition for an optical diffraction by an AOM. On the other hand, the incident angle of the 9.27 μm beam is adjusted at 28.89 mrad (= 38.55 mrad x 2 - 33.72 mrad) so that the output angle would be the same as the output angle of the 10.6 μm beam. Though the incident angle of 9.27 μm is not optimum for its diffraction condition, reducing the output beam power somewhat, two laser beams can be made coaxial after the AOM and the shift frequencies are identical. Figure 5 shows frequency spectra of beat signals ; (a) the reference signal, (b), (c) probing signals of 10.6 μm and 9.27 μm interferometers. These signals were obtained at monitor-out terminals in Fig. 3 without a plasma discharge. Our measurement indicated that all signals have the same center frequency of 2 MHz (1.99614 MHz is a more exact value). The difference is observed only in the shape of the spectrum. The reference signal has a relatively narrow spectrum with FWHM of 0.02 MHz. On the other hand, the probing signal shows a broader spectrum with FWHM of 0.11 MHz. This difference in spectrum width is supposed to originate from the diffraction characteristics on the AOM modulator for actual laser beams.

4. Operation Results

In this section three operation results are presented. They were obtained under operational conditions such as ; " free running laser mode without the retardation optics ", " free running laser mode with the retardation optics " and " stabilized laser mode with the retardation optics ". From the experience of the previous system (see fig. 5(a) in ref. [2]), the mode of " stabilized laser mode without the retardation optics " was not operated. It is because of the feedback action of the piezo transducer used to cause a serious frequency shift with a time scale of a second. This frequency shift results in phase shifts which cannot be eliminated.

Comparison of results in three operating conditions elucidates the performance of the interferometer.

4.1 Case 1 : free running laser mode without retardation optics

Figure 6 shows typical waveforms obtained for the L mode experiment under " the free running laser mode without retardation optics ". Plasma parameters are as follows; the plasma current ; I_p = 3 MA at the flat top, the toroidal magnetic field ; B_t = 4 T, the plasma major radius; R_p = 3.36 m, and the minor radius; a_p = 0.9 m, respectively. The neutral beam heating power ; P_{NB} and the ion cyclotron range heating power ; P_{IC} are shown in Fig. 6 (a). An ohmic coil current; I_F and the vertical field coil current; I_V are shown in Fig. 6 (b). Line electron densities at different radii measured by two channel alcohol laser interferometers are shown in Fig. 6 (c). The channel 2 looks along a chord closer to the plasma center than the channel 1. The peak line density observed at 6.4 sec is 1.0 x 10^{20} m^{-2} along the path of 2.74 m in the plasma. The line averaged electron density is 3.65 x 10^{19} m^{-3}. Figures 6 (d) and (e) show the phase shift signals of the CO_2 interferometers. Both have traces similar to each other strongly depending on I_V rather than I_F. Vertical field coils are closest to the reflection mirror at the vacuum window. This means that the phase shift mainly comes from the mechanical displacement of the diagnostic stage where the mirror mount rod is installed. A characteristic oscillation of the mirror mount rod is also observed on traces with a frequency of about 12 Hz. Figure 6 (f) indicates the line electron density of the dual CO_2 system

calculated by eq.(1) from the phase shifts of Fig. 6 (d) and (e). The line density data is averaged over 5 msec. In this plasma the time trace of the line density of the dual CO_2 system is similar to that of the channel 2 of the alcohol interferometer shown in Fig. 6 (c). The peak value of the CO2 interferometer is 2.3 x 10^{20} m^{-2}. As the path length of the tangential chord in the plasma is 5.82 m, the line-averaged density measured by the CO_2 system is about 3.95 x 10^{19} m^{-3}. This value is a little bit higher than the density of the alcohol interferometer. This is explained by the enhancement of the central density for the tangential chord. In this case, a density profile evaluated by a parabolic function fitting for the three line density data shows a flat shape with a parabolic power of 0.24.

The line density of 2.3 x 10^{20} m^{-2} corresponds to 0.26 fringes of the phase difference between the 10.6 μm and 9.27 μm interferometers. These small phase shifts are well extracted from total phase shift of a hundred fringes. It is concluded that the dual CO_2 laser interferometer is capable of the path length compensation.

Concerning the phase shift due to fluctuation of the lasing frequency, the large path difference of about 100 m is disadvantageous. Figure 7 shows the same data of Fig. 6 (f) without data averaging. In fig. 7 (a), the trace looks thick with periodic spikes with a frequency of about 200 Hz and an amplitude of around 5 x 10^{19} m^{-2}(see Fig. 7 (b)). Use of retardation optics eliminates this oscillation (the result will be explained in the coming subsection), suggesting that the oscillation comes from the fluctuation of the lasing frequency. Substituting l_1 = 100 m, l_2 = 2 m, $l_3 = l_4$ = 0 m, $\Delta\omega_B$ = 0 into the equation (8) in ref.7, we obtain the fluctuation amplitude of the frequency ; $\Delta\omega_p$ is estimated as order of 10^6 rad/sec, which corresponds to about 160 kHz.

4.2 Case 2 : free running laser mode with retardation optics

This operational mode is expected to be the most reliable. Figure 8 shows a result for a radio frequency wave (LHRF and ICRF) injection experiment. Plasma parameters are as follows; I_p = 2 MA, B_t = 4 T, R_p = 3.45 m, and a_p = 1.01 m, respectively. The line density shown in Fig. 8 (f) (averaged over 5 msec) looks smoother than the trace of Fig. 7 (f). Actually, the trace shown in Fig. 9 (a) is very quiescent without averaging and the fluctuation

amplitude is about $2 \times 10^{19} \, m^{-2}$. The 200 Hz oscillation is significantly reduced as shown in Fig. 9 (b). It almost disappeared from the trace. The dominant component of the fluctuation is the bit noise of the phase comparator. The retardation optics works effectively to extract the best performance of the interferometer. In this discharge a Thomson scattering measurement is available and three electron density profiles are obtained. Line densities calculated by re-integration along the CO_2 path from Thomson profiles are plotted in Fig. 8 (f) with closed circles, showing good agreement.

4.3 Case 3 : stabilized laser mode with retardation optics

In the case of continuous free running, a good longitudinal mode of the oscillator is terminated after several hours operation due to the thermal change of the cavity length. It is enough life time to measure a fifteen second pulse of the JT-60U operation, however, long discharge durations of future machines requires more stability. The stabilized laser mode is one of the attractive candidates when the retardation optics is available. Figure 10 shows the data obtained under this condition. At t =7 second the plasma current ; I_p = 1.2 MA, B_t = 1.6 T at the center, R_p = 3.51 m, and a_p = 0.87 m, respectively. No additional heating is applied to the plasma. It is clearly indicated that the frequency stabilization influences little on the density trace in Fig. 11. The density resolution is not degraded in comparison with data of free running mode shown in Fig. 9. By this result the stabilized laser mode is demonstrated to be suitable for long duration operations in future machines.

5. Example of data for major disruption

At the major disruption, it is often difficult to measure the electron density by conventional far infrared alcohol laser interferometers. A rapid change of the electron density or the large density gradient prevents reliable phase detection. The previous 10.6 μm and 3.39 μm combination system is also used to suffer from the fringe loss of the 3.39 μm signal due to a large mechanical vibration and displacement of mirrors at the disruption. These problems become more serious with an increase in the disruption speed. In contrast to

amplitude is about 2×10^{19} m^{-2}. The 200 Hz oscillation is significantly reduced as shown in Fig. 9 (b). It almost disappeared from the trace. The dominant component of the fluctuation is the bit noise of the phase comparator. The retardation optics works effectively to extract the best performance of the interferometer. In this discharge a Thomson scattering measurement is available and three electron density profiles are obtained. Line densities calculated by re-integration along the CO_2 path from Thomson profiles are plotted in Fig. 8 (f) with closed circles, showing good agreement.

4.3 Case 3 : stabilized laser mode with retardation optics

In the case of continuous free running, a good longitudinal mode of the oscillator is terminated after several hours operation due to the thermal change of the cavity length. It is enough life time to measure a fifteen second pulse of the JT-60U operation, however, long discharge durations of future machines requires more stability. The stabilized laser mode is one of the attractive candidates when the retardation optics is available. Figure 10 shows the data obtained under this condition. At t =7 second the plasma current ; I_p = 1.2 MA, B_t = 1.6 T at the center, R_p = 3.51 m, and a_p = 0.87 m, respectively. No additional heating is applied to the plasma. It is clearly indicated that the frequency stabilization influences little on the density trace in Fig. 11. The density resolution is not degraded in comparison with data of free running mode shown in Fig. 9. By this result the stabilized laser mode is demonstrated to be suitable for long duration operations in future machines.

5. Example of data for major disruption

At the major disruption, it is often difficult to measure the electron density by conventional far infrared alcohol laser interferometers. A rapid change of the electron density or the large density gradient prevents reliable phase detection. The previous 10.6 μm and 3.39 μm combination system is also used to suffer from the fringe loss of the 3.39 μm signal due to a large mechanical vibration and displacement of mirrors at the disruption. These problems become more serious with an increase in the disruption speed. In contrast to

the systems mentioned above, the dual CO_2 combination is more reliable and it succeeded in measuring the density of fast disruptions. Figure 12 shows an electron density behavior obtained at a high l_i disruption with a characteristic decay time of plasma current defined by Ip/(dIp/dt) [8] of 11 ms. The sampling rate of the density is 10 μs. The data is not smoothed. The electron density is 0.32×10^{20} m^{-2} before the energy quench. It rises to 3.4 times larger value as 1.1×10^{20} m^{-2} just before the start of current decay. Finally, it reaches the highest value of 9.6×10^{20} m^{-2} after multiple density spikes. It takes 5 ms after the first spike. An initial increase rate of the density is as fast as about 150 μs in this case.

6. Basic performance of ultra high resolution phase comparator

The phase resolution of the present comparator is 1/100 fringe, which corresponds to a line electron density of about 2×10^{18} m^{-2}. The effective density resolution, however, is reduced significantly in the dual CO_2 combination due to the very close wavelengths. The reduction factor for a two color scheme is (1 - 1/x) [2], here x is the ratio of two wavelengths. Therefore the reduction factor becomes 0.125 for dual CO2 system (x = 10.6/9.27), which means that the effective phase resolution for the density measurement is 1/12.5 fringe. This corresponds to a relatively poor resolution of a line density of about 1.6 $\times 10^{19}$ m^{-2}, which agrees with the observed resolution shown in section 4.2.

To improve the density resolution, a ultra high resolution phase comparator has been developed. The phase resolution is originally designed as $1/10^4$ fringe for the 2 MHz signal, which corresponds to a time resolution of 50 ps [2]. This specification depends on the discrimination accuracy of the high speed phase measuring module in the comparator. Figure 13 shows an examination set up of the module. A test signal generated by a synthesized oscillator is divided into two signals. One signal is for direct input as a reference signal and another is an input as a probing signal via a variable electrical delay line. When the delay line lengths is changed by a step, the measured time difference change between both signals indicates the accuracy of the time discrimination. Measured time differences are plotted against the delay line length in Figure 14. The test frequency is 1 MHz and the number of

the systems mentioned above, the dual CO_2 combination is more reliable and it succeeded in measuring the density of fast disruptions. Figure 12 shows an electron density behavior obtained at a high l_i disruption with a characteristic decay time of plasma current defined by $Ip/(dIp/dt)$ [8] of 11 ms. The sampling rate of the density is 10 μs. The data is not smoothed. The electron density is 0.32×10^{20} m^{-2} before the energy quench. It rises to 3.4 times larger value as 1.1×10^{20} m^{-2} just before the start of current decay. Finally, it reaches the highest value of 9.6×10^{20} m^{-2} after multiple density spikes. It takes 5 ms after the first spike. An initial increase rate of the density is as fast as about 150 μs in this case.

6. Basic performance of ultra high resolution phase comparator

The phase resolution of the present comparator is 1/100 fringe, which corresponds to a line electron density of about 2×10^{18} m^{-2}. The effective density resolution, however, is reduced significantly in the dual CO_2 combination due to the very close wavelengths. The reduction factor for a two color scheme is (1 - $1/x$) [2], here x is the ratio of two wavelengths. Therefore the reduction factor becomes 0.125 for dual CO2 system ($x = 10.6/9.27$), which means that the effective phase resolution for the density measurement is 1/12.5 fringe. This corresponds to a relatively poor resolution of a line density of about 1.6 $\times 10^{19}$ m^{-2}, which agrees with the observed resolution shown in section 4.2.

To improve the density resolution, a ultra high resolution phase comparator has been developed. The phase resolution is originally designed as $1/10^4$ fringe for the 2 MHz signal, which corresponds to a time resolution of 50 ps [2]. This specification depends on the discrimination accuracy of the high speed phase measuring module in the comparator. Figure 13 shows an examination set up of the module. A test signal generated by a synthesized oscillator is divided into two signals. One signal is for direct input as a reference signal and another is an input as a probing signal via a variable electrical delay line. When the delay line lengths is changed by a step, the measured time difference change between both signals indicates the accuracy of the time discrimination. Measured time differences are plotted against the delay line length in Figure 14. The test frequency is 1 MHz and the number of

sampling is 1000, respectively. One step of the delay line length is 0.5 cm which corresponds to 20 ps. It is found that the time difference is well discriminated for each case. The jitters of measured times are also an important index. Figure 15 shows a histogram of independent measurements for 10,000 sampling. An another fixed length delay line is used for this test. The standard deviation is obtained as 30 ps. Standard deviations for data shown in fig. 14 are also the same as 30 ps. From these results, it is concluded that the accuracy of the high speed phase measuring module is determined by the jitters with the standard deviation of 30 ps, which satisfies the designed value.

The new phase comparator has been assembled and an initial measurement for an actual plasma is planned early 1995. This new comparator will enable more precise analysis of the fast density change.

7. Discussion

As described in section 2, two AOMs provide a 2 MHz beat signal. The ultra high resolution phase comparator can measure input signals with a frequency range from 10 kHz to 50 MHz. Therefore a 40 MHz beat signals is directly acceptable and only one commercial AOM is sufficient for the heterodyne detection. An electrical frequency converter from 40 MHz to 2 MHz can also reduce the number of AOM. It is expected that the interferometer will become more stable by this kind of simplification of the AOM system.

A design of a multi-chordal interferometer for future large devices must face a port limitation issue. Vertical or tangential ports which have a pair of windows at each side of a vacuum vessel are suitable to minimize the influence from the darkening and the vibration of reflection mirrors. If reflection mirrors must be installed inside of the vacuum vessel to provide sufficient number of diagnostic chords, the dual CO_2 combination is one of the possible candidates. Its unique ability of the vibration compensation at the infrared radiation range is an advantage point. The relatively high lasing power, the simple configuration and easiness of obtaining required hardwares are also attractive.

sampling is 1000, respectively. One step of the delay line length is 0.5 cm which corresponds to 20 ps. It is found that the time difference is well discriminated for each case. The jitters of measured times are also an important index. Figure 15 shows a histogram of independent measurements for 10,000 sampling. An another fixed length delay line is used for this test. The standard deviation is obtained as 30 ps. Standard deviations for data shown in fig. 14 are also the same as 30 ps. From these results, it is concluded that the accuracy of the high speed phase measuring module is determined by the jitters with the standard deviation of 30 ps, which satisfies the designed value.

The new phase comparator has been assembled and an initial measurement for an actual plasma is planned early 1995. This new comparator will enable more precise analysis of the fast density change.

7. Discussion

As described in section 2, two AOMs provide a 2 MHz beat signal. The ultra high resolution phase comparator can measure input signals with a frequency range from 10 kHz to 50 MHz. Therefore a 40 MHz beat signals is directly acceptable and only one commercial AOM is sufficient for the heterodyne detection. An electrical frequency converter from 40 MHz to 2 MHz can also reduce the number of AOM. It is expected that the interferometer will become more stable by this kind of simplification of the AOM system.

A design of a multi-chordal interferometer for future large devices must face a port limitation issue. Vertical or tangential ports which have a pair of windows at each side of a vacuum vessel are suitable to minimize the influence from the darkening and the vibration of reflection mirrors. If reflection mirrors must be installed inside of the vacuum vessel to provide sufficient number of diagnostic chords, the dual CO_2 combination is one of the possible candidates. Its unique ability of the vibration compensation at the infrared radiation range is an advantage point. The relatively high lasing power, the simple configuration and easiness of obtaining required hardwares are also attractive.

8. Summary

The dual CO_2 laser interferometer has been developed for large tokamaks. The combination of different wavelength oscillators of 10.6 µm and 9.27 µm are utilized to simultaneous measurement of the electron density and the optical path components. A single AOM is commonly used for different wavelength lasers as the key technique to stabilize the system.

Several data show the basic performance of the dual CO_2 interferometer under the different operational modes. The dual CO_2 system can measure the electron density of 3 MA plasmas in the case of JT-60U. The observed effective density resolution is 2×10^{19} m^{-2}, which is determined by the phase resolution of the present phase comparator. It is presented that the stabilized laser mode with retardation optics is suitable for long duration discharges. The electron density behavior of fast major disruptions is successfully measured without a fringe loss.

The ultra high resolution phase comparator has been developed to improve the density resolution of the dual CO_2 interferometer. The phase resolution is designed as $1/10^4$ fringe for the 2 MHz signal or the accuracy of 50 ps, which is 100 times better than that of the present one. The achieved accuracy is 30 ps. The study of a fast density change is significantly improved by use of the dual CO_2 system.

Through this work, the feasibility of the dual CO_2 interferometer is well demonstrated for future large machines such as ITER.

Acknowledgement

References

[1] ITER Tokamak Device, ITER Documentation Series, No. 25 (IAEA, 1991) Vienna.

[2] Y. Kawano, A. Nagashima, S. Ishida, et al., Rev. Sci. Instrum. 63 (1992) 4971.

[3] Y.Kawano, T. Hatae, A. Nagashima, et al., JAERI-M report 93-057 (1993) 351.

[4] T. Nishitani, S. Ishida, M. Kikuchi, et al., Nucl. Fusion 34 (1994) 1069.

[5] M. Mori, S. Ishida, T. Ando, et al., Nucl. Fusion 34 (1994) 1045.

[6] T. Kondoh and the JT-60 Team, Phys. Plasmas 1 (1994) 1489.

[7] T. Fukuda and A. Nagashima, Rev. Sci. Instrum. 60 (1989) 1080.

[8] R. Yoshino, Y. Neyatani, N. Hosogane, et al., Nucl. Fusion 33 (1993) 1599.

Acknowledgement

References

[1] ITER Tokamak Device, ITER Documentation Series, No. 25 (IAEA, 1991) Vienna.

[2] Y. Kawano, A. Nagashima, S. Ishida, et al., Rev. Sci. Instrum. 63 (1992) 4971.

[3] Y.Kawano, T. Hatae, A. Nagashima, et al., JAERI-M report 93-057 (1993) 351.

[4] T. Nishitani, S. Ishida, M. Kikuchi, et al., Nucl. Fusion 34 (1994) 1069.

[5] M. Mori, S. Ishida, T. Ando, et al., Nucl. Fusion 34 (1994) 1045.

[6] T. Kondoh and the JT-60 Team, Phys. Plasmas 1 (1994) 1489.

[7] T. Fukuda and A. Nagashima, Rev. Sci. Instrum. 60 (1989) 1080.

[8] R. Yoshino, Y. Neyatani, N. Hosogane, et al., Nucl. Fusion 33 (1993) 1599.

(a)

(b)

(c)

Fig.1 Laser beam line in the vacuum vessel. (a) top view of the JT-60U vacuum vessel with the laser path in the case of a large plasma configuration, (b) cross sectional view in the case of a relatively large plasma configuration, (c) cross sectional view in the case of the high βp configuration, respectively. Vertical chords of ch. 1 and ch. 2 are used for the alcohol laser interferometer.
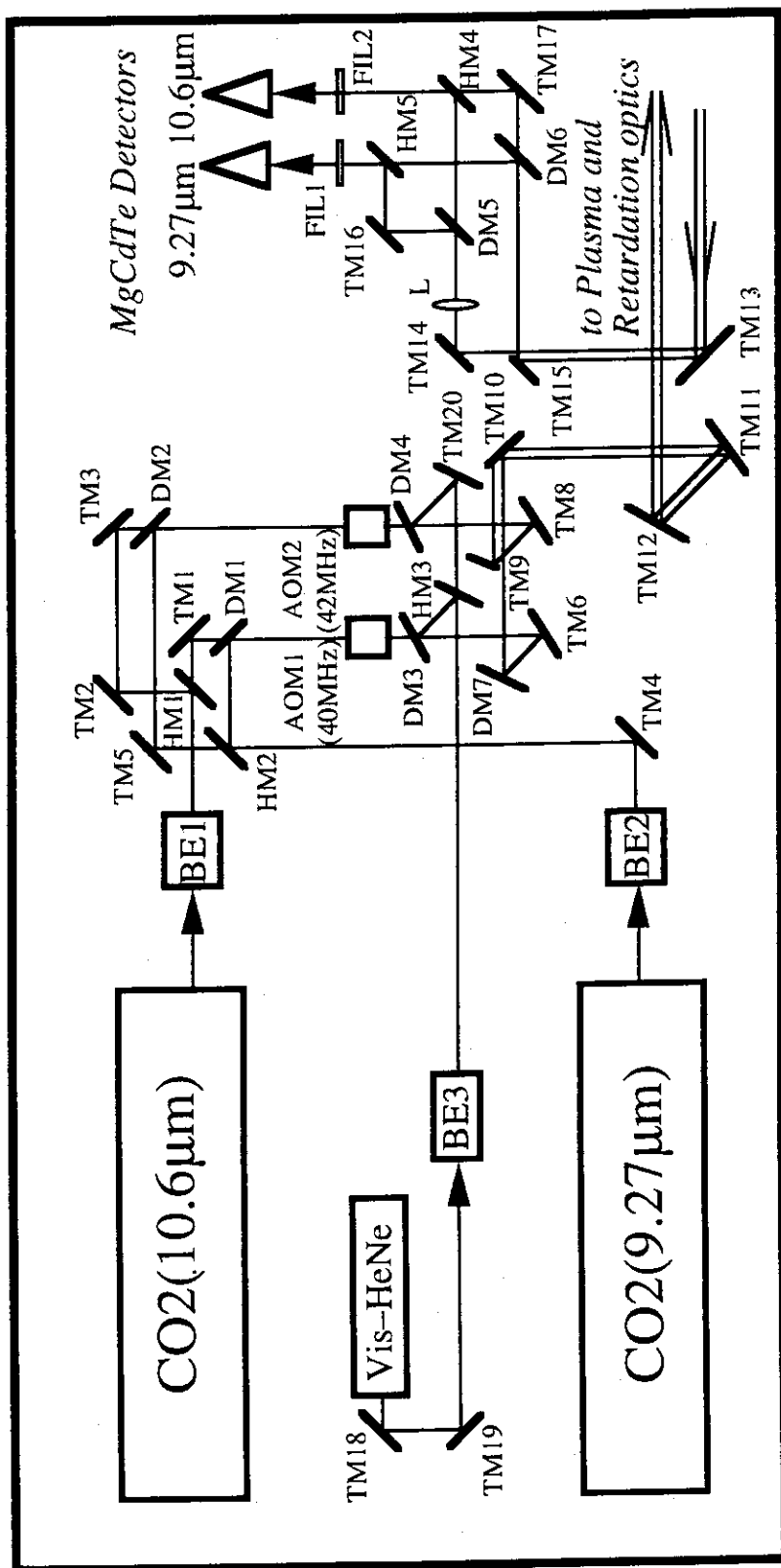
Fig.2 Layout of optical components on the vibration isolated bench. Two CO₂ oscillators are tuned for different branches as 10P(20)(10.6μm) and 9R(20) (9.27μm). Visible-HeNe laser is used for an alignment of optical components. BE ; beam expanders to modify laser beam parameters so as to propagate in relay optics. TM ; total reflection mirror. HM ; half mirror. DM ; dichromatic mirror working as a reflector for only 9.27μm. FIL1 ; filter for propagating a 9.27 μm laser beam and for cutting a 10.6 μm beam. FIL2 ; filter for propagating a 10.6 μm laser beam and for cutting a 9.27μm beam. L ; lens. AOM ; acoust-optic-modulator head as the frequency shifter for the heterodyne detection.
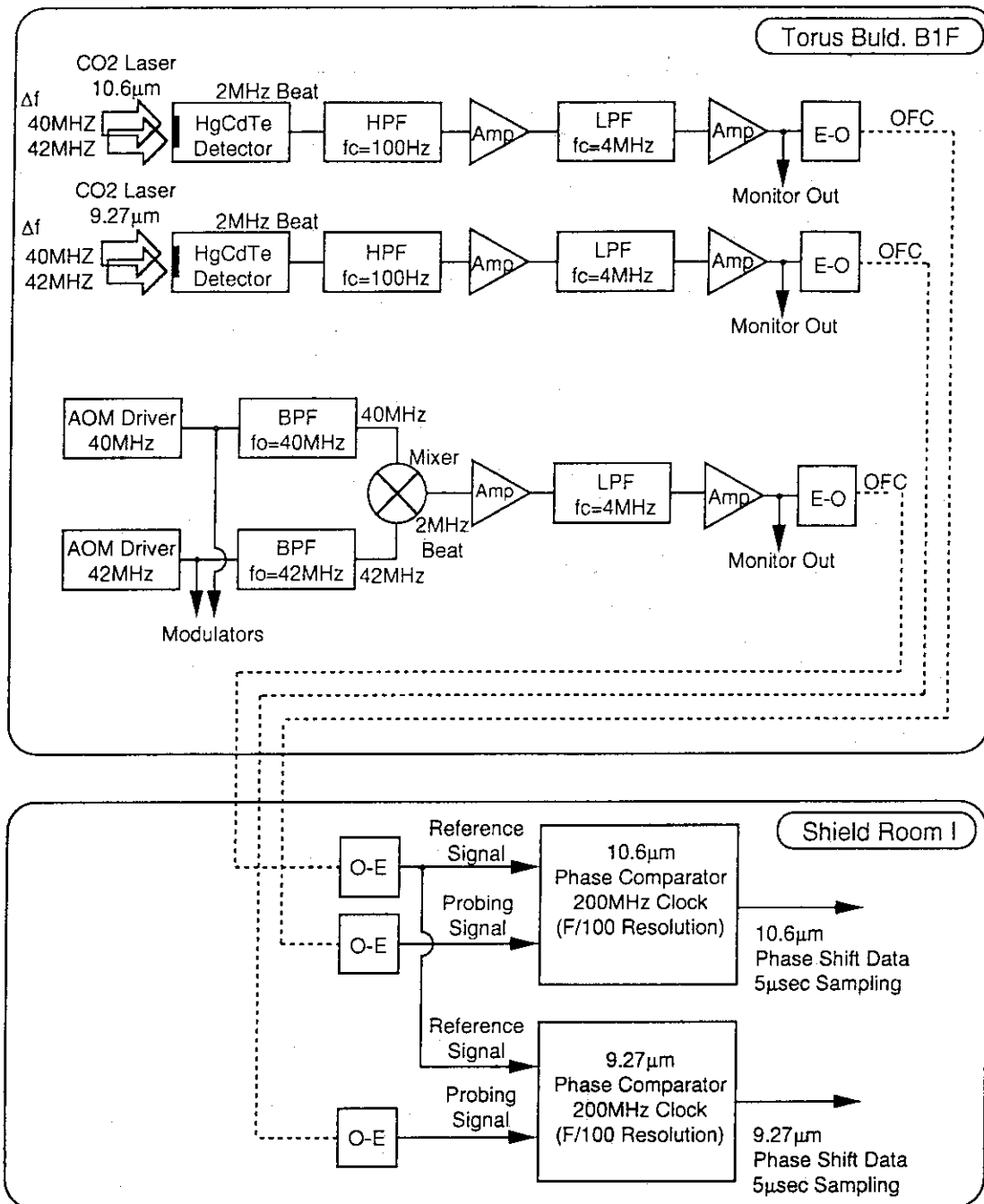
Fig.3 Schematic of the signal detection and the data acquisition. Signal
detection part consists of two same probing branch and a reference branch.
Each interference light is detected by a HgCdTe detector. High pass
filter, low pass filter and pre-amplifiers are used to produce a probing
beat signal. Reference beat signal is generated from AOM driver signals
by an electrical frequency mixing. This signal is commonly used for both
of 10.6 μm and 9.27 μm interferometers. Data acquisition part consists
of phase comparators with 1/100 fringe resolution, the data storage system
and the main frame computer(ISP computer). The maximum sampling rate is
determined by the data storage system as 5 μs.
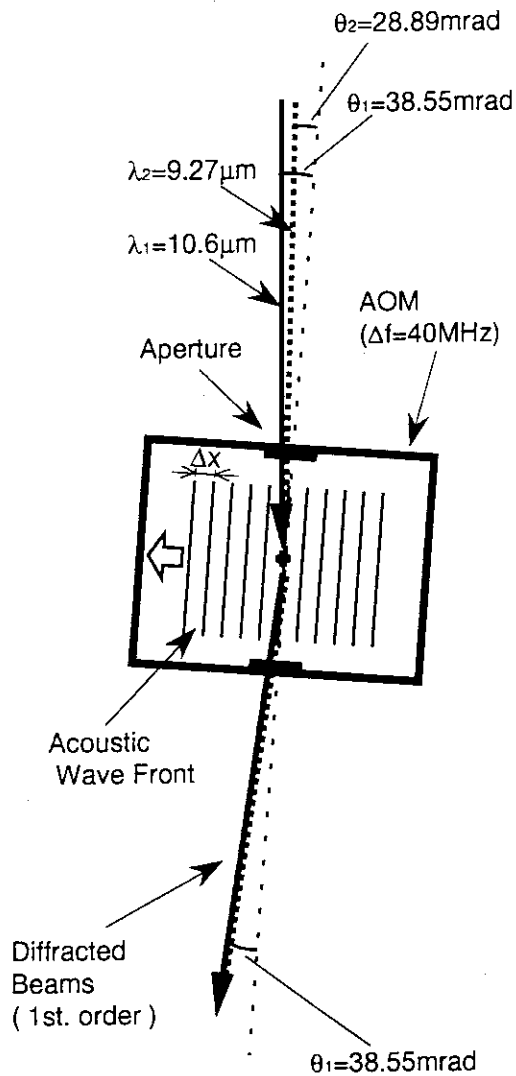
Fig.4 Alignment of the common use of an AOM for different wavelength CO_2 beams. Incident angles are adjusted so that output beams of 10.6 μm and 9.27 μm are coaxially propagated.
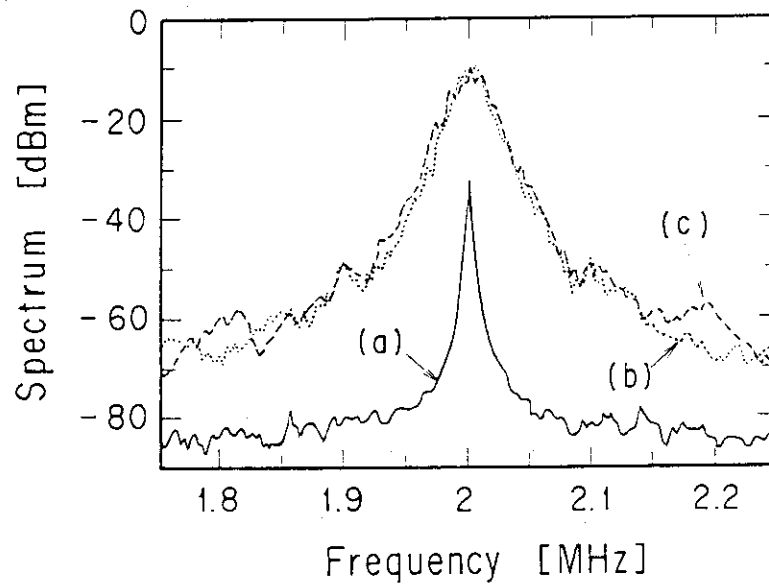
Fig.5 Frequency spectrum of 2 MH$_z$ beat signals. (a) reference beat signal,
(b) beat signal of 10.6 μm, and(c)beat signal of 9.27 μm, respectively.
Measured center frequencies are same as 1.99614 MH $_z$ for three signals.
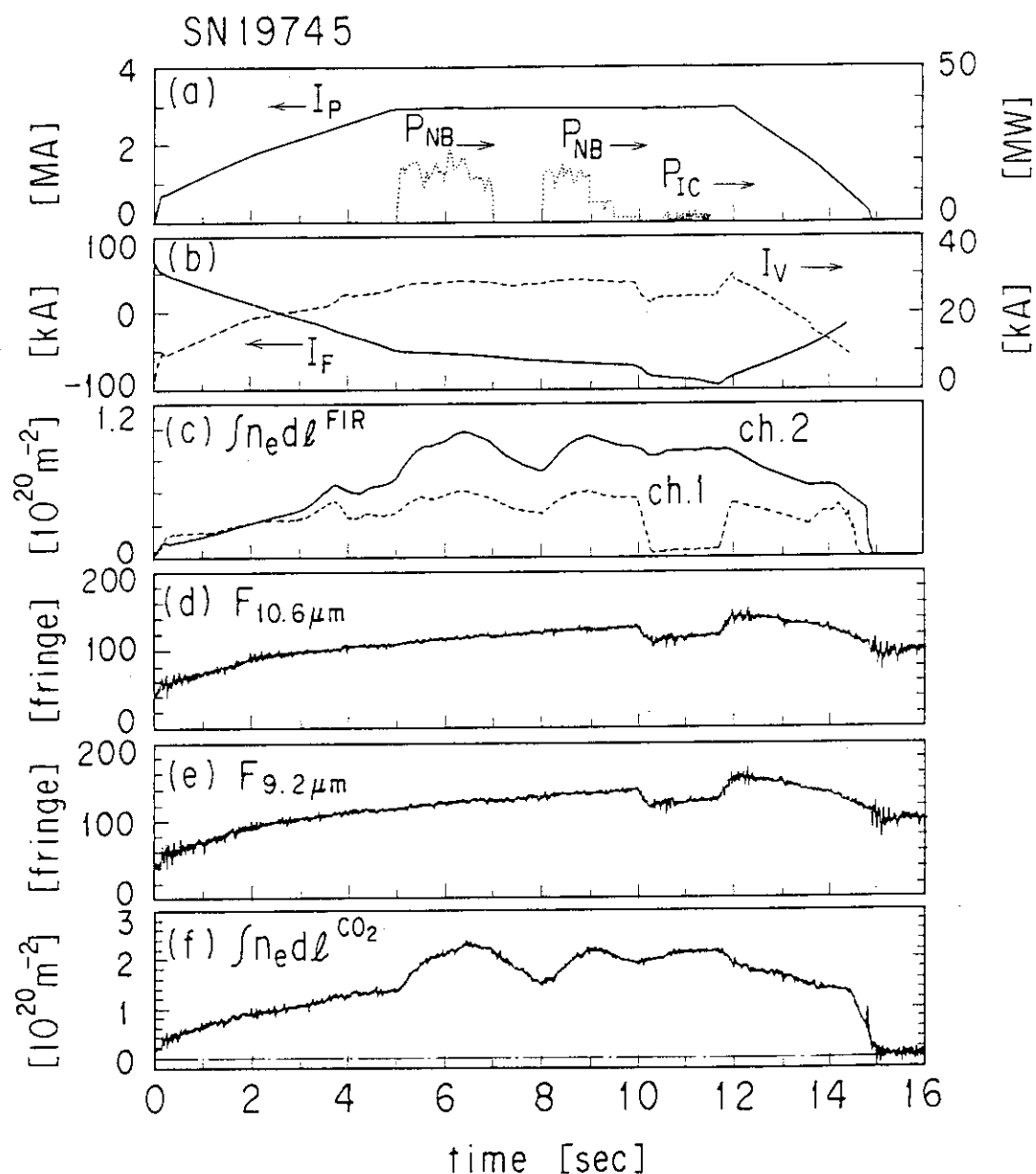
Fig.6 Typical waveforms obtatined under "free running laser mode without retardation optics ". (a) plasma current and additional heating power, (b) ohmic coil current and vertical field coil current, (c) line electron density measured by the two channel alcohol laser interferometer, (d) phase signal of 10.6μm interferometer, (e) phase signal of 9.27μm interferometer, and (f) line electron density measured by the dual CO_2 laser interferometer with every 5 msec averaging, respectively.
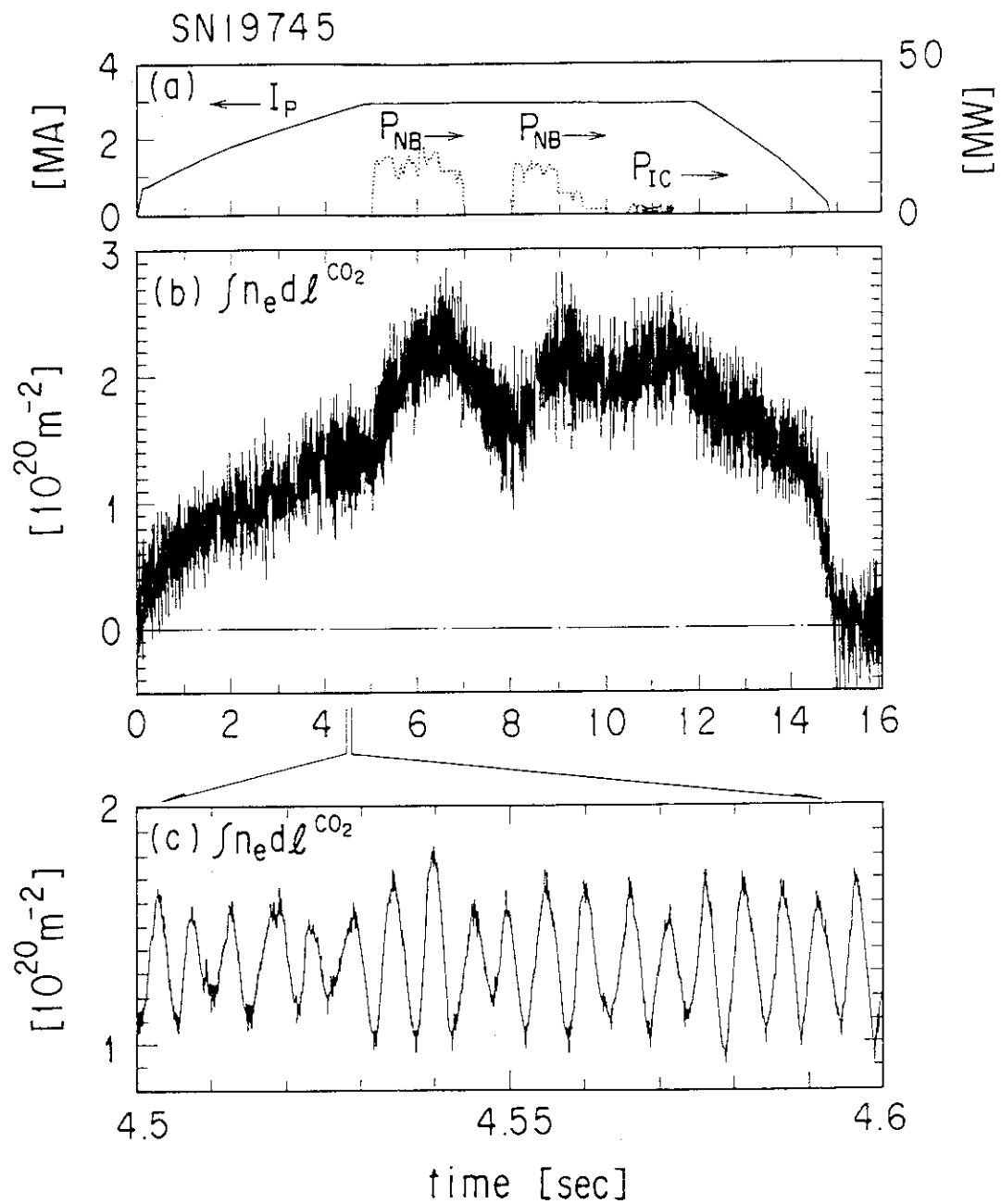
Fig.7 Line electron density without averaging. The data is identical to Fig.6 (f). Density resolution is determined by the periodic noise component with the frequency of 200Hz and the amplitude of $5 \times 10^{19} m^{-2}$.
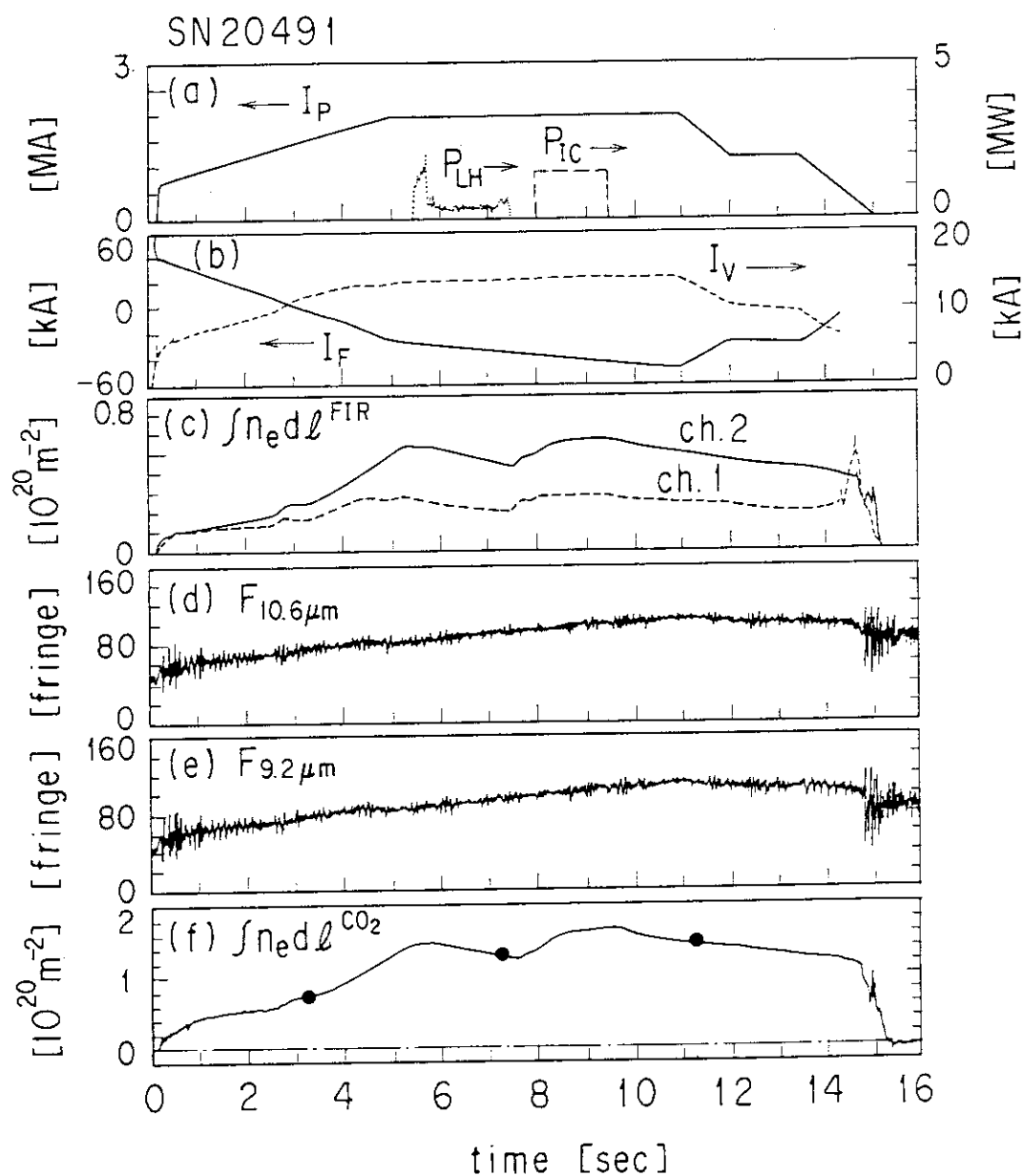
Fig.8 Typical waveforms obtained under "free running laser mode with retardation optics". Closed circles in fig.8(f) are re-integrated line densities along the CO₂ laser chord from density profiles measured by Thomson scattering system.
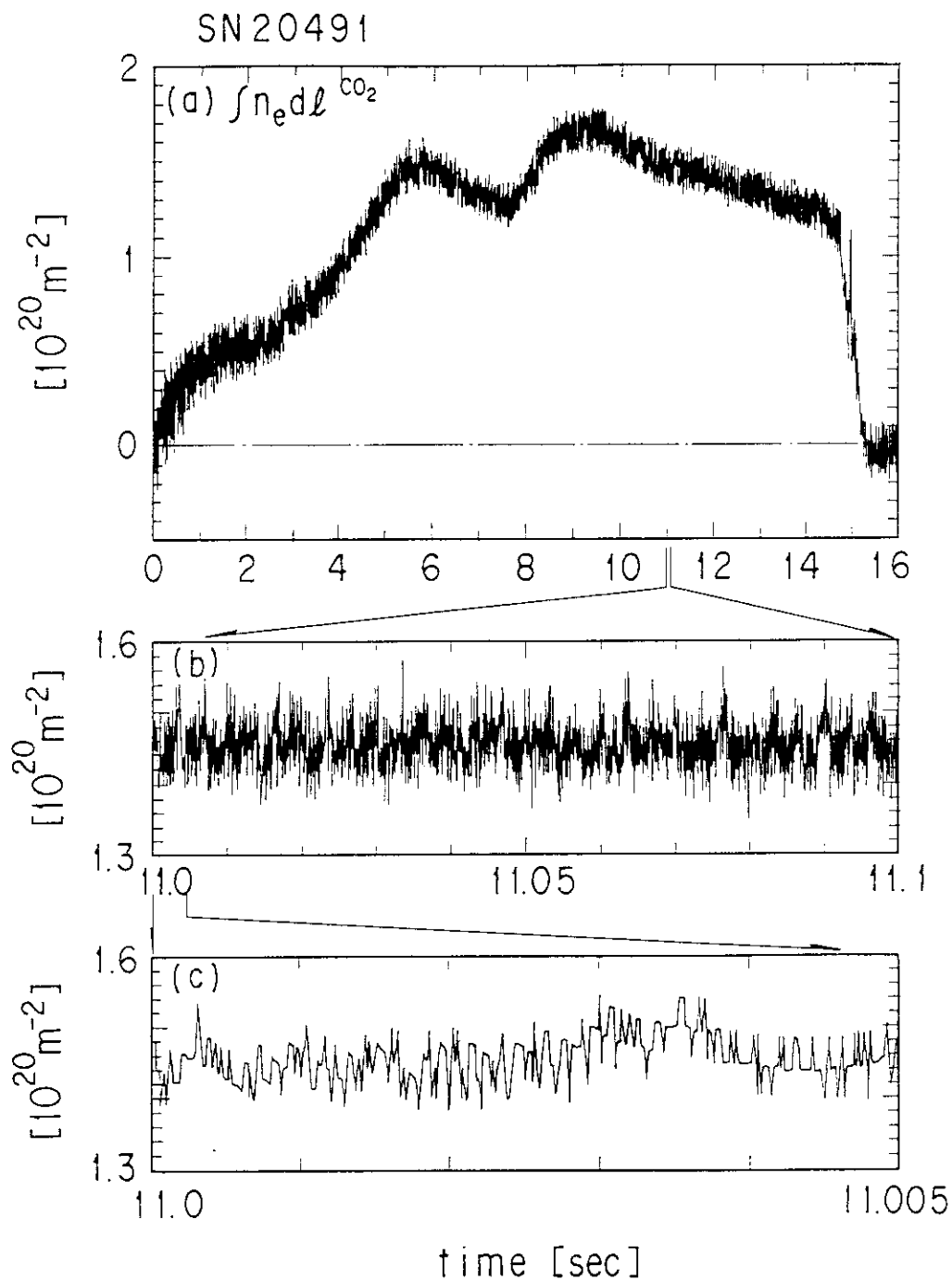
Fig.9 Line electron density without averaging. The data is identical to Fig.8
(f). The periodic noise component seen in Fig.7 is eliminated. Density
resolution is determined by the bit noise of the phase comparator as about
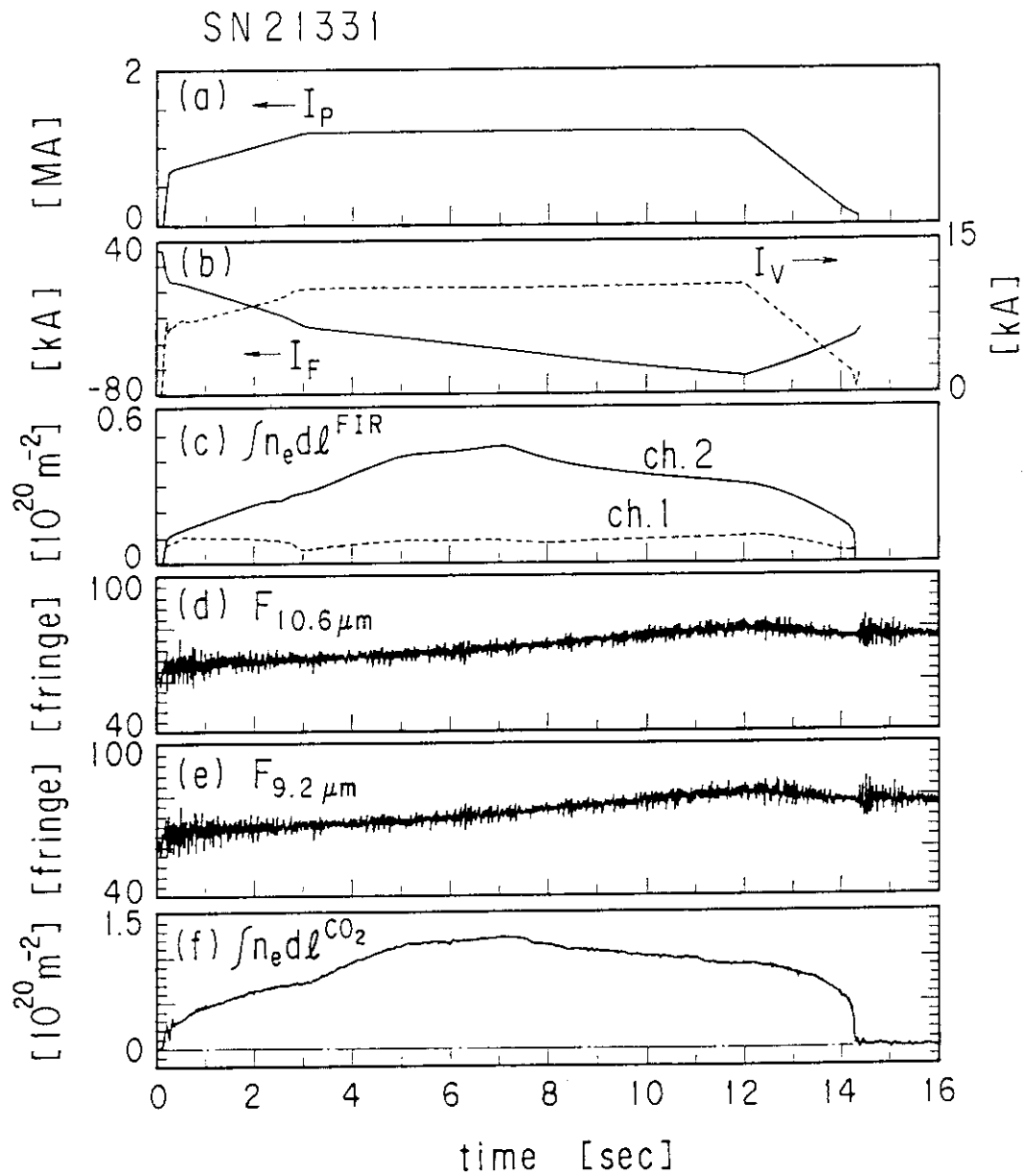$2 \times 10^{18} m^{-2}$.

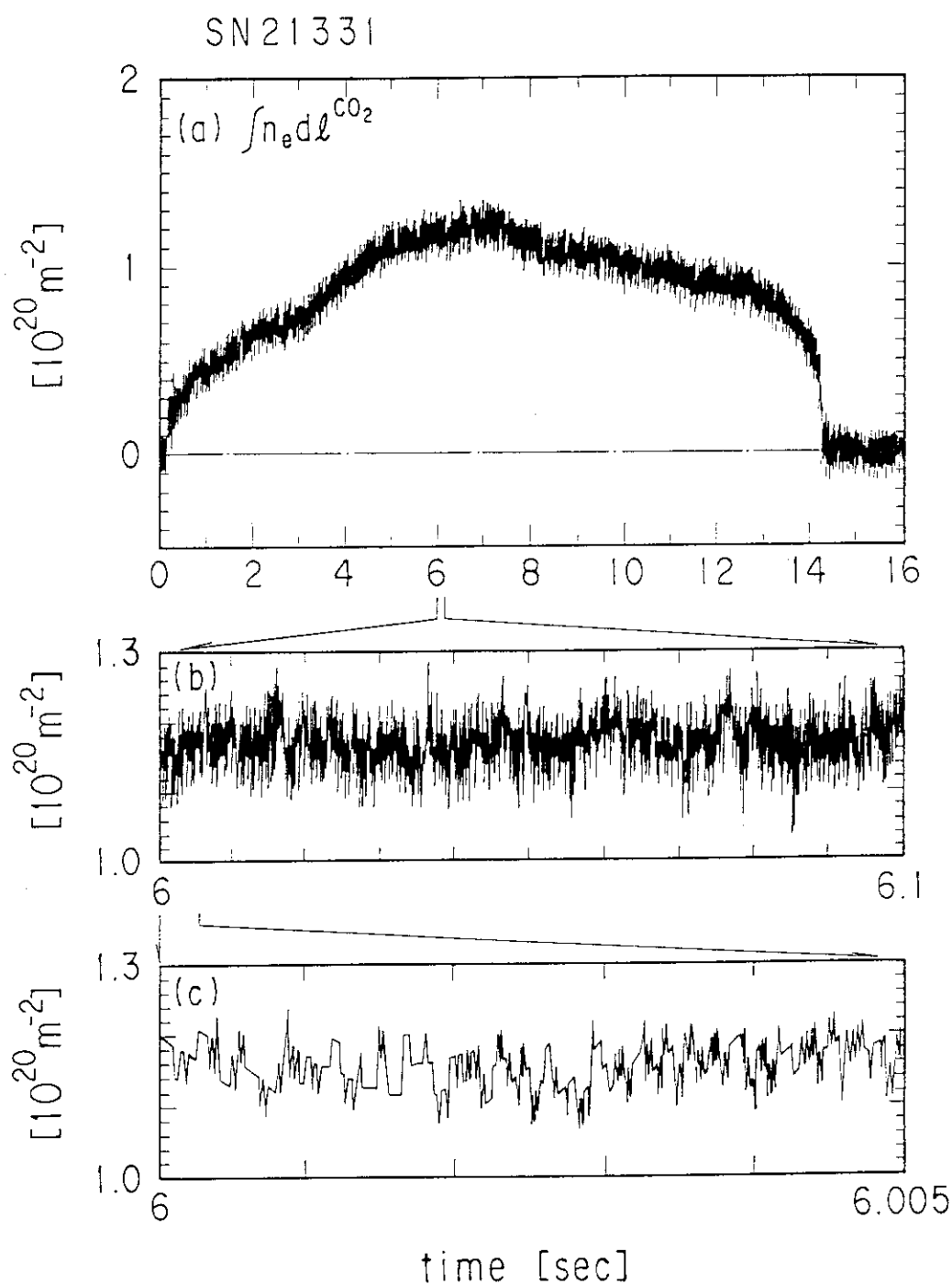Fig.10 Typical waveforms obtained under "stabilized laser mode with retardation optics ".

SN21331

Fig.11 Line electron density without averaging. The data is indentical to Fig.10(f). Influence of frequency stabilization is not recognized and the density resolution is not degraded in comparison with the trace of fig.9.
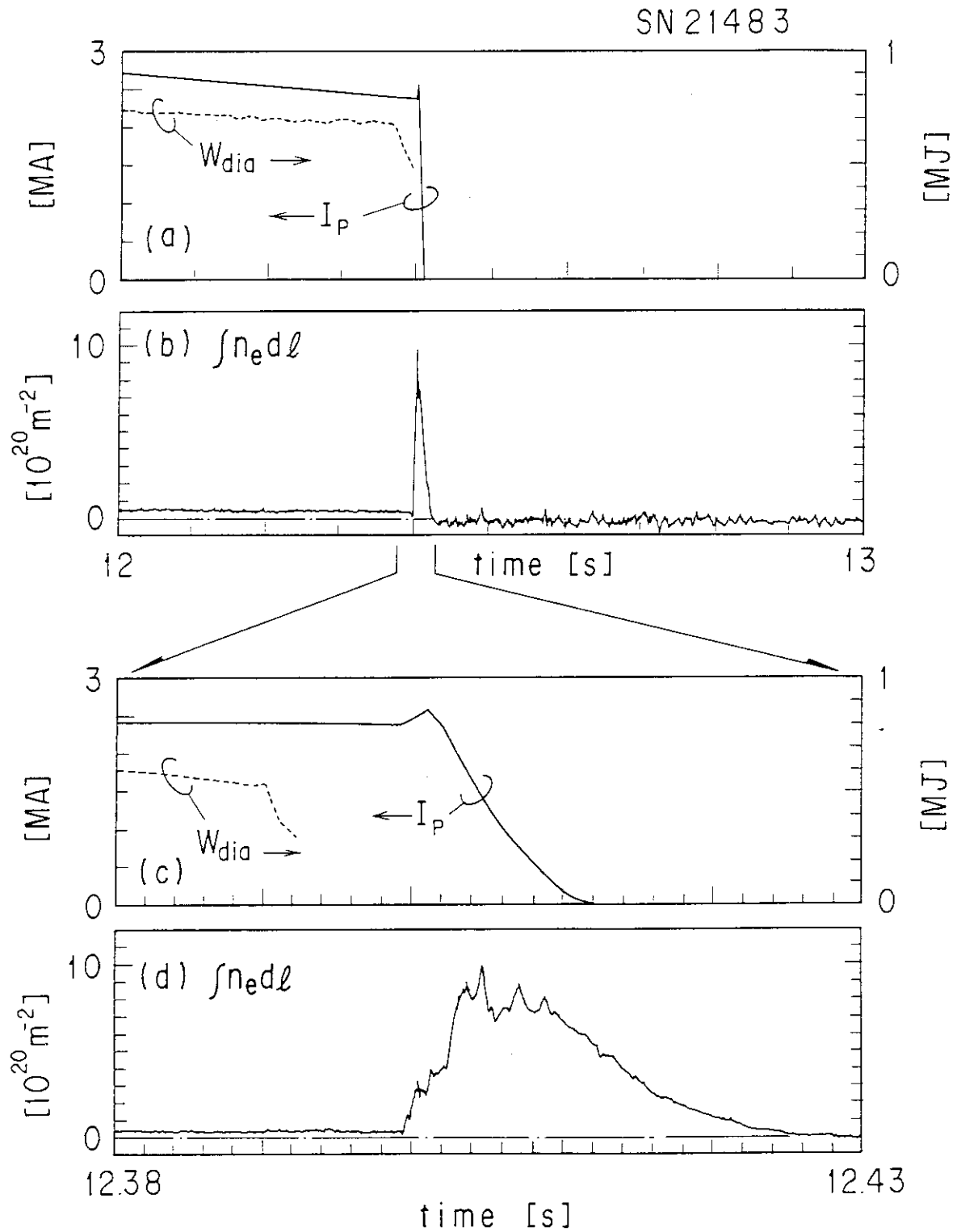
Fig.12 Electron density behavior of a high l_i disruption with the current
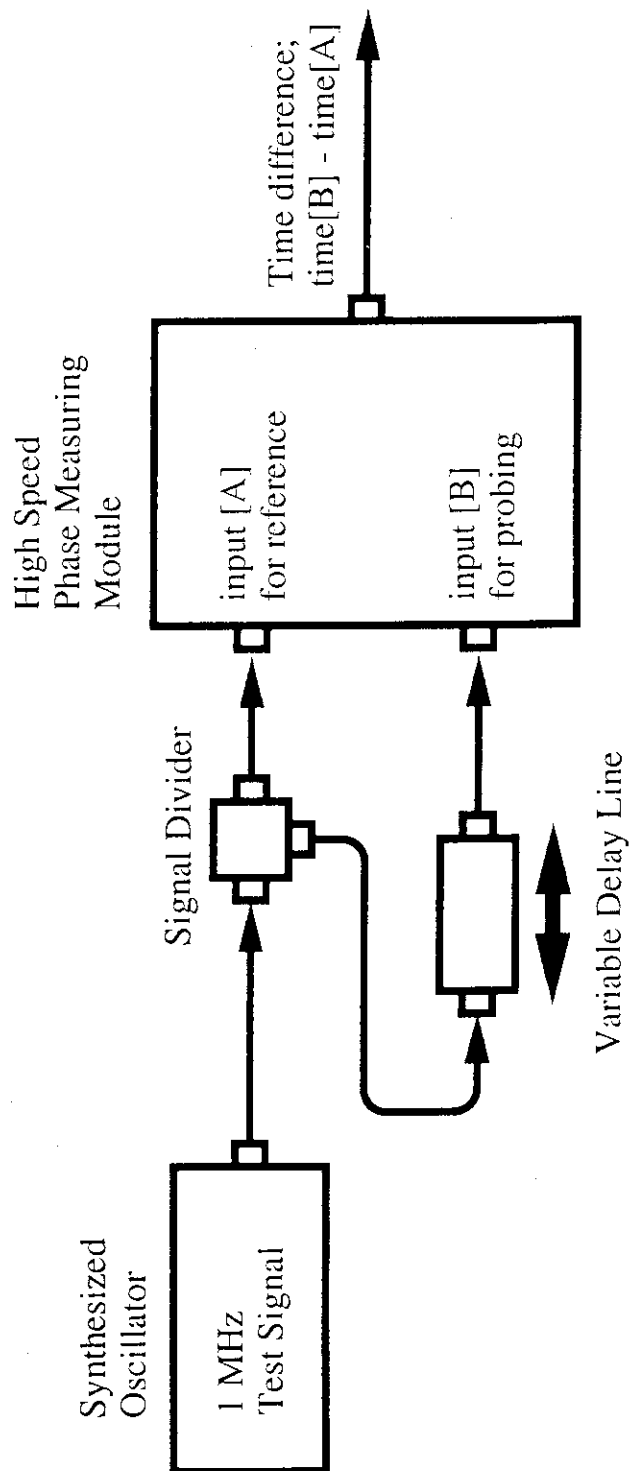decay time Ip/(dIp/dt)of 11 msec.

Fig.13 Arrangement to test the high speed phase measuring module. Time difference between input [A] and input [B] is measured. Test frequency is 1 MHz. Variable delay line is used to change the arrival timing of the probing signal for input [B].
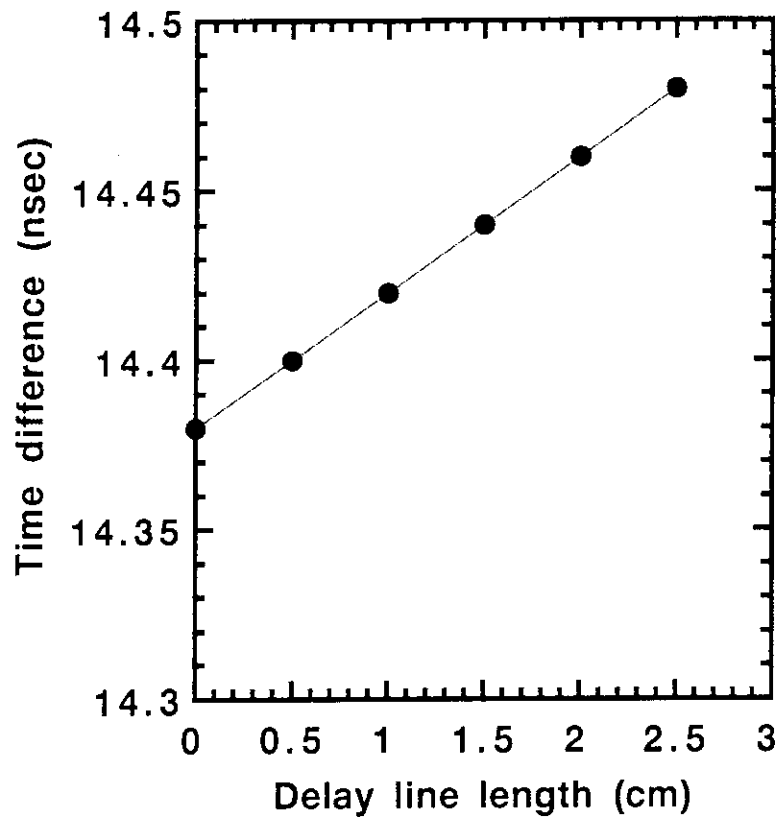
Fig.14 Measured time differences against the delay line length. Each number of sampling is 1,000. Time difference of 20 ps is well discriminated.
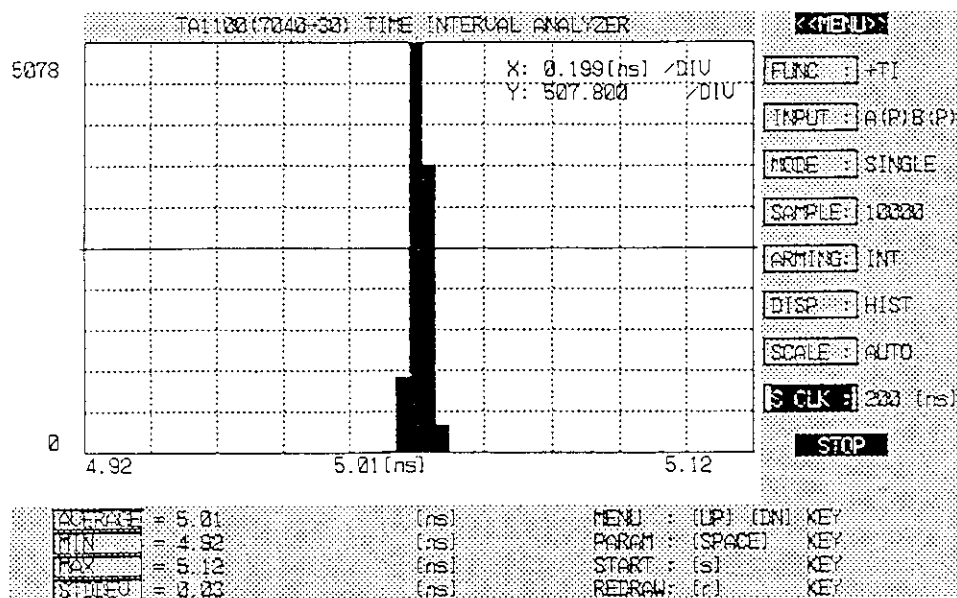

Fig.15 Histogram of the time difference data of 10,000 samples. Fixed length line is used. The average time is 5.01 ns and the standard deviation of 10,000 data is obtained as 30 ps.